Regulation of planar growth by the *Arabidopsis* AGC protein kinase UNICORN

Balaji Enugutti[a], Charlotte Kirchhelle[a], Maxi Oelschner[a], Ramón Angel Torres Ruiz[b], Ivo Schliebner[c], Dario Leister[c], and Kay Schneitz[a,1]

[a]Entwicklungsbiologie der Pflanzen and [b]Lehrstuhl für Genetik, Wissenschaftszentrum Weihenstephan, Technische Universität München, 85354 Freising, Germany; and [c]Lehrstuhl für Molekularbiologie der Pflanzen (Botanik), Department Biologie I, Biozentrum, Ludwig-Maximilians-Universität München, 82152 Planegg-Martinsried, Germany

Edited* by Elliot M. Meyerowitz, California Institute of Technology, Pasadena, CA, and approved August 1, 2012 (received for review March 27, 2012)

The spatial coordination of growth is of central importance for the regulation of plant tissue architecture. Individual layers, such as the epidermis, are clonally propagated and structurally maintained by symmetric cell divisions that are oriented along the plane of the layer. The developmental control of this process is poorly understood. The simple cellular basis and sheet-like structure of *Arabidopsis* integuments make them an attractive model system to address planar growth. Here we report on the characterization of the *Arabidopsis UNICORN* (*UCN*) gene. Analysis of *ucn* integuments reveals localized distortion of planar growth, eventually resulting in an ectopic multicellular protrusion. In addition, *ucn* mutants exhibit ectopic growth in filaments and petals, as well as aberrant embryogenesis. We further show that *UCN* encodes an active AGC VIII kinase. Genetic, biochemical, and cell biological data suggest that UCN suppresses ectopic growth in integuments by directly repressing the KANADI transcription factor ABERRANT TESTA SHAPE. Our findings indicate that *UCN* represents a unique plant growth regulator that maintains planar growth of integuments by repressing a developmental regulator involved in the control of early integument growth and polarity.

AGC protein kinase | growth suppression | floral development | ovule | signal transduction

Plant tissue morphogenesis depends on the coordination of cellular behavior within tissue layers. The formation of distinct layers depends on asymmetric cell division, the developmental control of which is under intense investigation (1, 2). After initiation, individual cell layers are propagated by symmetric cell divisions (3) with division planes often oriented along the plane of the layer (planar growth). For example, the layered structure of the epidermis is maintained by anticlinal cell divisions, whereas periclinal cell divisions are usually suppressed (4). Division planes of symmetrically dividing cells can be accurately predicted by a mathematical rule linking cell geometry and cytoskeletal dynamics (5), and much progress has been made in the elucidation of the cellular machinery controlling the division plane of dividing plant cells. However, developmental controls that maintain the planar orientation of symmetrical cell divisions within a tissue layer remain poorly understood (3).

Arabidopsis integuments represent an attractive model to study tissue morphogenesis. They are lateral determinate tissues of the ovule, the progenitors of the seed coat, and undergo a regular mode of development resulting in simple tissue architecture. An inner and an outer integument originate from the epidermis of the central chalaza (6, 7). They grow into laminar extensions with each integument consisting of a bilayered sheet of anticlinally dividing cells. The outer integument eventually develops into a hood-like structure that envelops the distal nucellus carrying the developing embryo sac and the inner integument.

Coordination of symmetrical cell divisions along the plane of the extending integument represents an intriguing feature of integument development. However, with the exception of the two receptor-like kinase genes, *ACR4* and *ALE2* (8–10), none of the many genes affecting integument morphogenesis (11, 12) have been implied to play a primary role in the maintenance of the sheet-like organization of the integument cell layers. Thus, the signaling mechanisms regulating a central aspect of integument growth are poorly understood.

Here we show that *UNICORN* (*UCN*) regulates planar integument development by suppressing aberrantly oriented growth. In addition, *UCN* restricts growth in stamen filaments, petals, and cotyledons, and it affects the division planes in the proembryo. Our molecular characterization revealed that *UCN* encodes a functional AGC VIII kinase. Furthermore, we provide evidence that UCN regulates growth patterns in ovules by repressing the KANADI transcription factor ABERRANT TESTA SHAPE (ATS).

Results

Wild-Type Integument Development in *Arabidopsis*. Both integuments were initiated, in cross-section view, in single epidermal cells that underwent oblique or periclinal cell divisions (7). Further development resulted in bilayered sheets of cells that expanded within the plane of the integument and underwent anticlinal cell divisions (Fig. 1 *A–D*) (7, 13). The early oblique or periclinal cell divisions likely include asymmetric cell divisions because early differences in gene expression and morphology indicate that cells of the two cell layers rapidly adopt different fates (Fig. 1 *I* and *M*) (7, 14–17). Thus, each integument exhibits tissue polarity and consists of an upper, or adaxial, and lower, or abaxial, cell layer.

***UCN* Restrains Growth in Various Lateral Organs and the Embryo.** Integuments of the recessive *ucn-1* mutant (18) showed spontaneous local ectopic growths caused by aberrant changes in cell size, shape, and proliferation (Fig. 1 *E–H*). The earliest irregularities could be observed shortly after integument initiation (stage 2-IV/V; stages according to ref. 7) (Fig. 1*E*). In most ovules, however, the phenotype became apparent at slightly later stages (early stage 3 onward). At various positions along the integuments, one or a few cells in a cell layer of the inner or outer integument divided periclinally or sometimes obliquely (Fig. 1*G*). Similar aberrant cell divisions were observed at later stages as well. Furthermore, abnormally expanded cells could contribute to protrusion formation. However, not every aberrant cellular division seems to result in a protrusion. Generally, one outgrowth developed at a usually proximal integument position (18). Frequently, two protrusions, or occasionally three to four outgrowths, could be observed as well (Fig. 1 *F* and *H*). Protrusion formation on the inner integument did not depend on the

Author contributions: B.E., C.K., D.L., and K.S. designed research; B.E., C.K., M.O., and I.S. performed research; B.E., C.K., R.A.T.R., I.S., D.L., and K.S. analyzed data; and K.S. wrote the paper.

The authors declare no conflict of interest.

*This Direct Submission article had a prearranged editor.

Freely available online through the PNAS open access option.

[1]To whom correspondence should be addressed. E-mail: schneitz@wzw.tum.de.

This article contains supporting information online at www.pnas.org/lookup/suppl/doi:10.1073/pnas.1205089109/-/DCSupplemental.

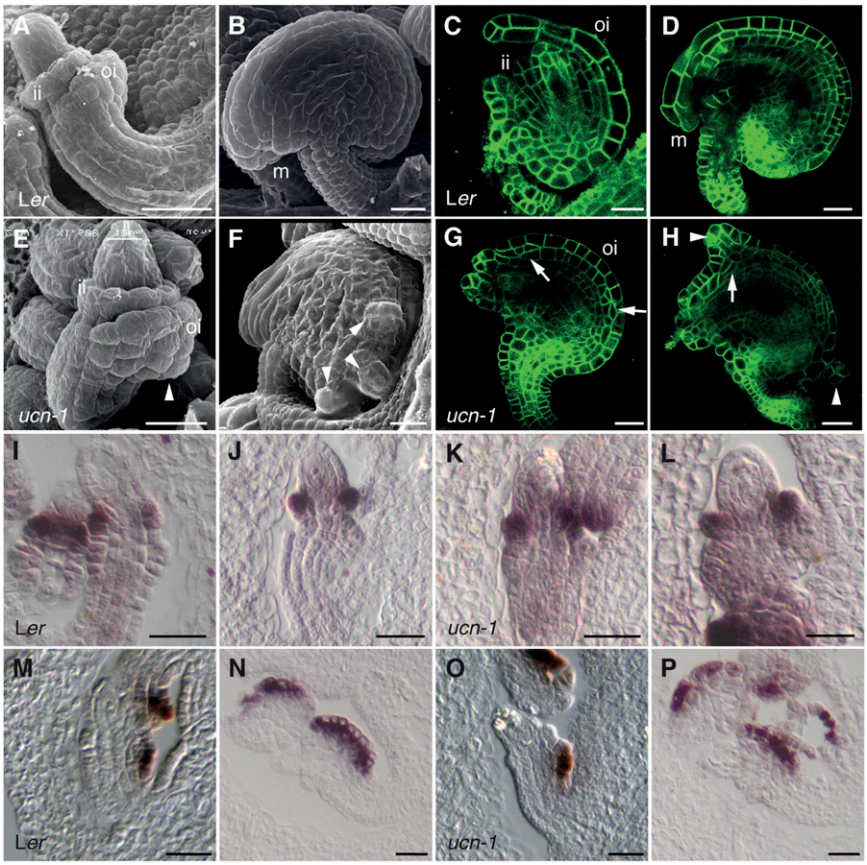

Fig. 1. Defective planar growth in *ucn-1* integuments. (*A* and *B*) Scanning electron micrographs (SEMs) of wild-type ovules. (*A*) Stage 2-IV. ii, inner integument; oi, outer integument. (*B*) Stage 4. m, micropyle. (*C* and *D*) Confocal micrographs of wild-type ovules expressing the plasma membrane marker *pUBQ::EGFP:LTI6B* (51). (*C*) Stage 3-I. (*D*) Early stage 4. (*E–H*) Ovules of *ucn-1*. A similar series to that in *A–D* is shown. (*E*) Early protrusion formation (arrowhead). (*F*) Protrusions (arrowheads). (*G* and *H*) Irregular cell divisions (arrows) and protrusions (arrowheads). (*I–L*) In situ hybridization on sectioned ovules using a *PHB* probe (16). (*I*) Stage 2-III wild-type ovule. Signal is detectable in the adaxial layer of the inner integument. (*J*) Stage 2-IV wild-type ovule. (*K* and *L*) *ucn-1*. Ovules of comparable stages as in *I* and *J* are depicted. Note the normal *PHB* expression. (*M–P*) In situ hybridization on sectioned ovules using an *INO* probe (16). Early stage 2-III and late stage 2-IV ovules, respectively, are depicted. *(M* and *N*) Wild-type. *INO* expression is restricted to the abaxial cell layer in the outer integument. (*O* and *P*) *ucn-1*. Normal spatial expression domain of *INO* is shown. (Scale bars: 20 μm.)

presence of an outer integument (*SI Appendix*, Fig. S1). Expression of the class III HD-ZIP gene *PHABULOSA* (*PHB*) (19), an early marker for the adaxial cell layer of the inner integument (16), was not altered in *ucn-1* ovules (Fig. 1 *I–L*; *SI Appendix*, Fig. S1). In addition, the abaxial layer of the outer integument of *ucn-1* exhibited normal spatial expression of the abaxial cell fate marker gene *INNER NO OUTER* (*INO*) (refs. 14 and 20; Fig. 1 *M–P*; *SI Appendix*, Fig. S1). The result suggests that outer integument cells contributing to the protrusions exhibited at least partial outer integument identity and did not represent callus. In addition, the data indicate that *UCN* does not affect the establishment of adaxial–abaxial polarity in integuments.

Further analysis revealed that stage 13 *ucn-1* stamen filaments showed prominent outgrowths (Fig. 2 *A* and *B*), as did the petals (Fig. 2 *C* and *D*), which were also folded. In rare cases, we detected protrusions on petioles of cotyledons as well (Fig. 2 *E* and *F*), which superficially resembled leaf petiole outgrowths caused by allelic incompatibilities at the *OAK* locus (21). In addition, *ucn-1* showed reduced fertility, and we observed aberrant cell divisions in ∼25% of embryos (Fig. 2 *J–L*; *SI Appendix*, Table S1). The asymmetric division of the zygote appeared normal in *ucn-1*. The first recognizable defect consisted of horizontal or oblique, rather than vertical, first and second symmetrical cell divisions in the proembryo. More advanced *ucn-1* embryos showed abnormal cell proliferation, apparently concentrated to the basal part of the embryo. Thus, *UCN* affects the division plane of symmetrically dividing cells in integuments and early embryos. To test whether cell-cycle regulation was affected in *ucn-1*, we assayed the expression of several core cell-cycle genes in petals. Indeed, *UCN* influenced the cell cycle because we found complex changes in their expression levels (*SI Appendix*, Fig. S2). Together, the results indicate that *UCN* restrains abnormal cell proliferation and growth in ovules, filaments, petals, embryos, and cotyledons.

***UCN* Encodes an AGC VIII Kinase.** Map-based cloning, isolation of multiple mutant alleles, and genomic rescue experiments (*SI Appendix*, Fig. S3 *A*, *B*, and *D*, Table S2, and *SI Materials and Methods*) identified *UCN* as At1g51170 (Fig. 3*A*), encoding a member of the plant-specific AGC VIII family of protein kinases (22–25). UCN is a functional kinase that can autophosphorylate *in trans* as well as transphosphorylate the general kinase substrate myelin basic protein (Fig. 3*B*). The *ucn-1* mutation resulted in the substitution of a conserved glycine at position 165 for a serine (G165S), which caused loss of kinase activity (Fig. 3*B*). UCN falls into the AGC2 subclass of the AGCVIII kinase family, which consists of two distantly related subclades with two members each (23). The closest relative of UCN (AGC2-3) is AGC2-4/At3g20830. UCN and AGC2-4 share 73% identity at the amino acid level, and thus AGC2-4 was renamed to UNICORN-LIKE (UCNL).

Detection of *UCN* expression in developing flowers by in situ hybridization or immunolocalization was unsuccessful, indicating

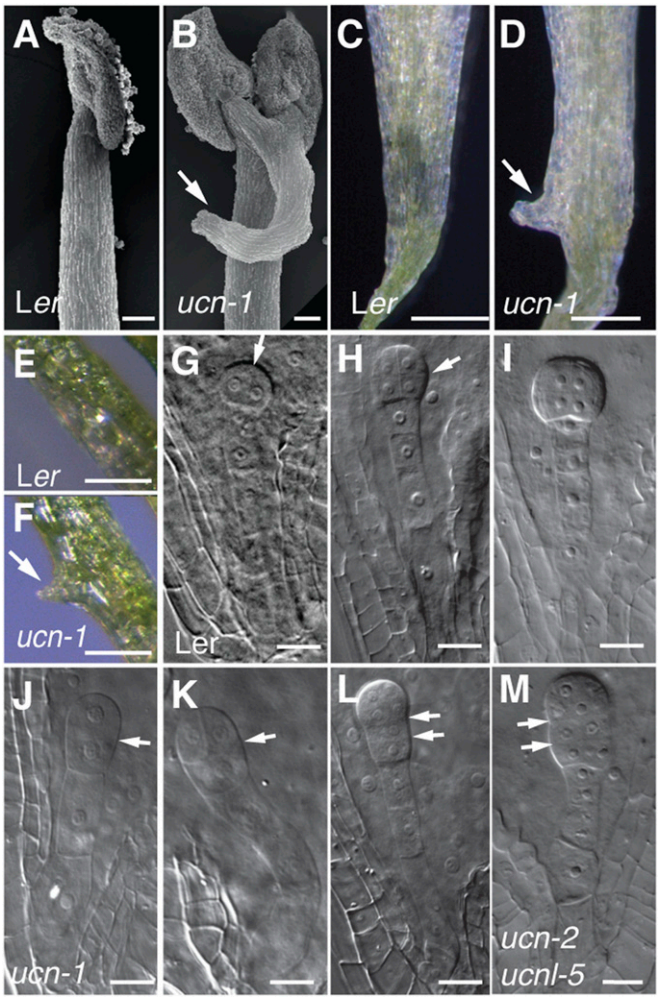

Fig. 2. Aberrant growth in floral organs, cotyledons, and embryos of *ucn-1* plants. (*A–D*) Floral defects (stage 13). (*A* and *B*) SEMs of stamens. (*B*) Protrusion on *ucn-1* filament (arrow). (*C* and *D*) Petals. (*D*) *ucn-1* petal with protrusion (arrow). (*E* and *F*) Cotyledons. (*F*) *ucn-1*. Note the protrusion (arrow). (*G–M*) Embryo defects in fertilized ovules (stage 12–14 flowers). (*G–I*) Wild type. (*G*) Proembryo with first vertical division (arrow). (*H*) Octant embryo after first horizontal division (arrow). (*I*) Globular embryo with protoderm formed. (*J–L*) *ucn-1*. Arrows indicate horizontal division planes. (*J*) Two-cell proembryo exhibiting aberrant horizontal division. (*K*) Proembryo (compare with *H*). (*L*) Proembryo with aberrant second horizontal division plane in the basal cell. (*M*) A mutant embryo in an ovule from a selfed *ucn-2/ucn-2 ucnl-5/+* parent (compare with *I*). Note the aberrant cell proliferation in the basal proembryo. (Scale bars: *A* and *B*, 50 μm; *C–F*, 0.5 mm; *G–M*, 20 μm.)

that *UCN* is expressed at very low levels. However, quantitative real-time PCR (qRT-PCR) revealed *UCN* expression at floral stages 8–11 (Fig. 3*C*), which encompasses the period when *ucn* phenotype first becomes apparent. The results also showed that *UCN* is normally transcribed in stage 8–11 *ucn-1* flowers but slightly higher in later stages (Fig. 3*C*).

To assess the subcellular localization of UCN, we performed bimolecular fluorescence complementation (BiFC) analysis (Fig. 3 *D–G*). The results indicated that full-length UCN can form homodimers in a plant cell, confirming results from the in vitro kinase assays. Furthermore, signals were broadly distributed throughout the cell, including the nucleus. Indeed, UCN carries a bipartite nuclear localization signal. Moreover, direct detection of endogenous UCN and UCNL protein (*SI Appendix*, Fig. S6) by using an anti-UCN antiserum revealed expression of UCN and/or UCNL in the epidermis and cortex of the transition zone of the root apex. Cells exhibited signal in the nucleus, the cytoplasm, and likely at the plasma membrane (Fig. 3 *H–J*). Computer prediction also suggested a chloroplast localization of UCN. However, the BiFC results (Fig. 3 *D–G*), as well as in vitro chloroplast import studies (*SI Appendix*, Fig. S3*E*) and chlorophyll fluorescence parameter measurements (*SI Appendix*, Table S3), failed to confirm this prediction. Together, the data indicate that UCN shows a broad subcellular distribution and may function in different cellular compartments.

***UCN* and *UCNL* Act Redundantly.** *UCN* is transcribed in *ucn-1* (Fig. 3*C*), and UCN_{G165S} protein may have residual biological activity. Furthermore, *UCN* and *UCNL* show a broad and overlapping expression profile (Fig. 3*C*; *SI Appendix*, Fig. S3*F*). In flowers, *UCNL* exhibited notably reduced transcript levels in comparison with *UCN* (Fig. 3*C*). Nevertheless, *UCN* and *UCNL* could act redundantly. Thus, we investigated the phenotype of *ucn* and *ucnl* null alleles as well as *ucn ucnl* double mutants. Two T-DNA insertion lines, *ucn-2* and *ucnl-5*, carry null alleles (*SI Appendix*,

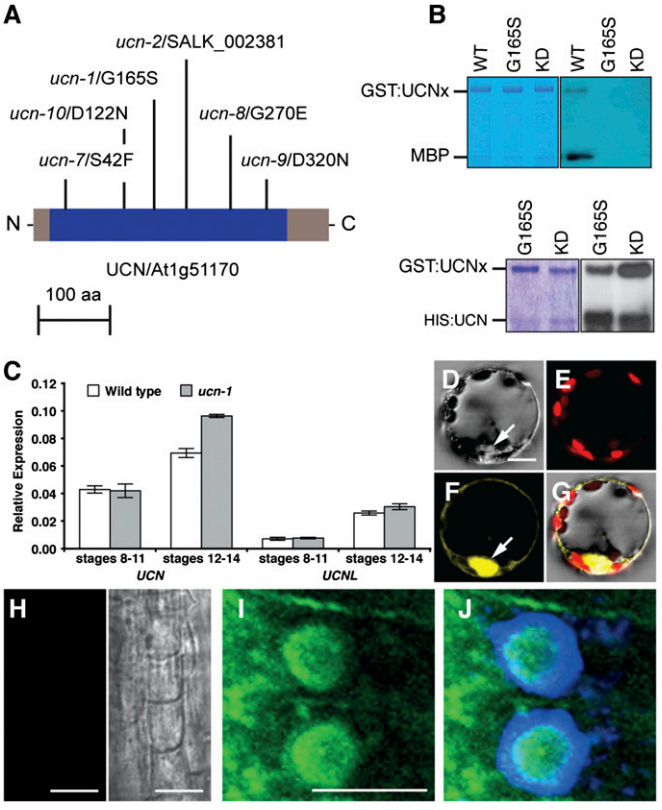

Fig. 3. UCN is an active AGC kinase and localizes to the cytoplasm and the nucleus. (*A*) Scheme of predicted UCN protein (blue, kinase domain). Mutations are indicated. aa, amino acids. (*B*) In vitro kinase assay with purified GST:UCN or HIS:UCN fusion proteins. (*Left*) Coomassie blue gel. (*Right*) Corresponding autoradiographs. GST:UCNx denotes different GST:UCN variants indicated on top. (*Upper*) Autophosphorylation and phosphorylation of myelin basic protein (MBP). $GST:UCN_{KD}$ (K55E mutation, negative control). (*Lower*) Autophosphorylation and transphosphorylation of unfunctional $GST:UCN_{G165S}$ or $GST:UCN_{KD}$ by HIS:UCN. (*C*) A qRT-PCR-based comparison of floral *UCN* (*Left*) and *UCNL* (*Right*) mRNA levels in wild type and *ucn-1*. (*D–G*) BiFC-visualization of UCN dimerization. Different views of a protoplast cotransfected with *pSPYNE:UCN* and *pSPYCE:UCN* plasmids are shown. (*D*) Bright-field view. (*E*) Chloroplast autofluorescence (red signal). (*F*) YFP channel (yellow signal). Arrow indicates nucleus. (*G*) Merge. Cotransfecting empty pUC-SPYNE/SPYCE plasmids did not result in signal (*SI Appendix*, Fig. S4). (*H–J*) Immunolocalization of UCN/UCNL in whole-mount roots of 6-d-old seedlings. (*H*) Preimmune serum (*Left*) and bright-field view (*Right*). (*I* and *J*) Anti-UCN antibody (*I*) plus DAPI (*J*). (Scale bars: *D–G*, 30 μm; *H–J*, 10 μm.)

Figs. S3 *B* and *C*, S5, and S6, Table S2, and *SI Materials and Methods*) but appeared phenotypically wild type. Upon selfing of a *ucn-2*/*ucn-2 ucnl-5*/+ plant, a total of 136 F1 plants were genotyped. Of those, 87 plants were heterozygous for *ucnl-5*, whereas 49 carried the wild-type *UCNL* allele, indicating that *ucn-2 ucnl-5* double mutants were embryo lethal with full penetrance. Furthermore, embryo aberrations were essentially identical to the embryo defects observed in *ucn-1* plants (Fig. 2 *J–M*; *SI Appendix*, Table S1). These results corroborate redundancy and reveal that complete loss of *UCN* and *UCNL* activity leads to fully penetrant embryo lethality. Interestingly, *ucn-1* plants showed the null phenotype with a reduced penetrance of ~25%, indicating that *ucn-1* is a hypomorph, at least with respect to embryo development. A simple explanation for this genetic behavior is to assume that UCN and UCNL bind to the same protein complex and that UCN, as well as the partially functional UCN_{G165S} protein, titrate out wild-type UCNL protein (*SI Appendix*, Fig. S7).

UCN Restrains Ectopic Growth in Integuments Through Negative Regulation of ATS. To address the mechanism of *UCN*-mediated ectopic growth suppression, we combined *ucn-1* with several ovule mutants (*SI Appendix*, Figs. S1*G* and S9). Interestingly, the phenotype of *ucn ats* double mutants suggested that *UCN* suppresses protrusion formation in integuments by negatively regulating *ATS* (Fig. 4 *A–D*). *ATS* encodes a putative transcription factor (15) of the KANADI (KAN) family (26, 27). Defects in *ats* mutants are specific to ovules, which show congenitally fused integuments (15, 28, 29). In wild-type ovules, *ATS* expression is observed at the boundary between the two initiating integuments, at the abaxial side of the inner integument and the adaxial side of the outer integument, and eventually becomes restricted to the abaxial cells of the inner integument (15) (Fig. 4 *I–J*). Interestingly, ovules of *ucn-1 ats-3* double mutants exhibited *ats*-like integuments that were essentially devoid of *ucn*-like protrusions (Fig. 4*D*; *SI Appendix*, Table S4). This result demonstrates that *ats* is epistatic to *ucn*. Moreover, it strongly suggests that *UCN* and *ATS* act in the same genetic pathway, that *UCN* is a negative regulator of *ATS*, and that *ATS* is the main direct or indirect downstream target of *UCN* in integument growth control.

We investigated how *UCN* regulates *ATS*. An ~45-fold increase in *ATS* expression levels within the normal *ATS* expression domain in the activation-tagging line *sk21-D* (30) resulted in

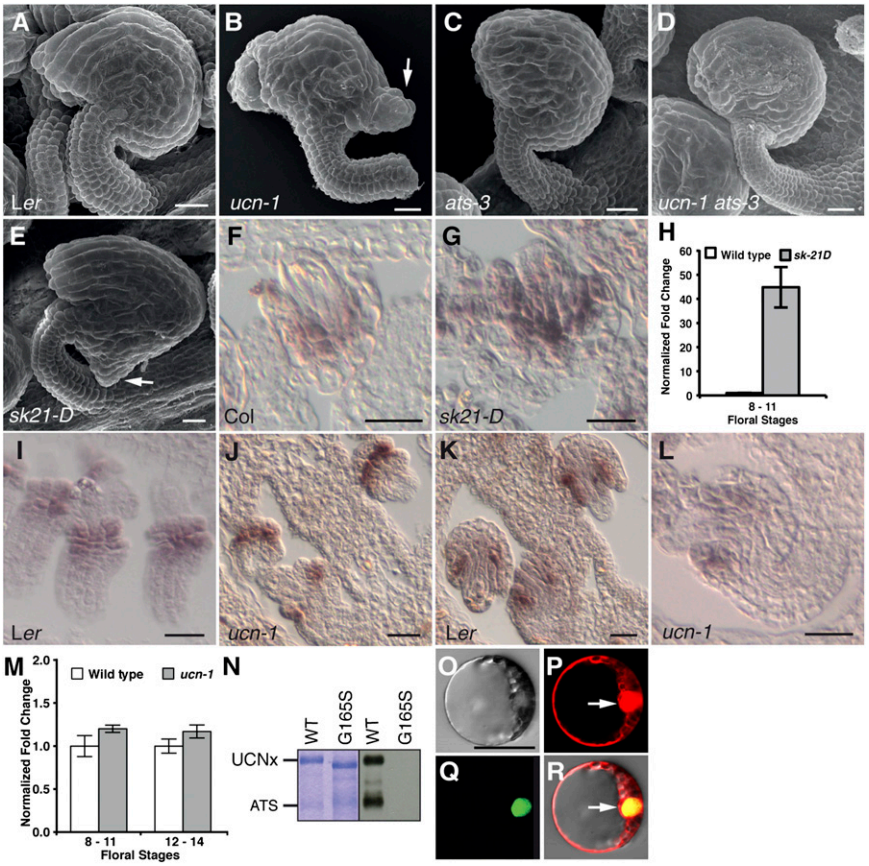

Fig. 4. *UCN* is a negative posttranscriptional regulator of *ATS*. (*A–E*) SEMs of early stage 4 ovules. (*A*) Wild type. (*B*) *ucn-1*. (*C*) *ats-3*. (*D*) *ucn-1 ats-3*. Note the absence of protrusions. (*E*) *ATS* activation tagging line *sk21-D*. Compare the protrusion with *B* (arrow). (*F* and *G*) Spatial *ATS* expression analyzed by in situ hybridization on sectioned ovules. Stage 2-IV wild-type (*Left*) and *sk21-D* (*Right*) ovules are shown. In wild type, detectable *ATS* expression ranges from the abaxial layer of the inner integument to the adaxial layer of the outer integument. *ATS* spatial expression appears normal in *sk21-D*. (*H*) Floral *ATS* mRNA levels in wild type and *sk21-D* measured by qRT-PCR. Note the high level of *ATS* expression at floral stages 8–11 in *sk21-D*. (*I–L*) Spatial *ATS* expression analyzed by in situ hybridization on sectioned ovules. (*I* and *J*) Stage 2-III wild-type (*Left*) and *ucn-1* (*Right*) ovules are shown. No changes were observed. (*K* and *L*) Stage 2-V wild-type (*Left*) and *ucn-1* (*Right*) ovules are shown. *ATS* expression is mainly observed in the inner integument. No changes were observed. (*M*) Floral *ATS* mRNA levels measured by qRT-PCR. No significant changes were observed. (*N*) In vitro kinase assay using purified GST:UCN and GST:ATS fusion proteins. (*Left*) Coomassie blue gel. (*Right*) Corresponding autoradiograph. UCNx denotes different GST:UCN variants indicated on top. (*O–R*) BiFC assay of UCN/ATS interaction. Different views of a protoplast cotransfected with *pSPYNE:ATS*, *pSPYCE:UCN*, and *pGY-1:mCherry* plasmids are shown. (*O*) Bright-field view. (*P*) Signal distribution of free mCherry. Arrow highlights the nucleus. (*Q*) YFP signal distribution indicating UCN/ATS interaction. (*R*) Merge. Cotransfecting of empty pUC-SPYNE/SPYCE plasmids did not result in signal (*SI Appendix*, Fig. S4). (Scale bars: *A–G* and *I–L*, 20 μm; *O–R*, 30 μm.)

a *ucn*-like protrusion in ovules (Fig. 4 *E–H*; *SI Appendix*, Fig. S8 and Table S4), corroborating the notion that negative regulation of *ATS* is essential for regular planar growth of integuments. However, *ATS* expression was found to be unaltered in *ucn-1* (Fig. 4 *I–M*), indicating that *UCN* regulates *ATS* posttranscriptionally. We thus explored whether the two proteins could interact physically. Although the low level of *UCN* expression in developing flowers precluded a direct test in planta, recombinant UCN phosphorylated ATS in in vitro kinase assays (Fig. 4*N*). Furthermore, we were able to show that the two proteins interacted in nuclei of plant cells in a BiFC assay (Fig. 4 *O–R*). These findings suggest that UCN may directly repress ATS protein activity in the nucleus, possibly through differential phosphorylation.

Discussion

Here we present evidence that *UCN* restrains aberrant growth in diverse plant organs. The *ucn* outgrowths are distinct from the wart-like epidermal cell swellings caused by several mutations in *Arabidopsis* and maize (31–33) or the multiplication of epidermal cell layers caused by the maize *Xcl1* mutation (34). Furthermore, *UCN* is likely to function in a different pathway than *ACR4* and *ALE2* (*SI Appendix*, Fig. S9 *M–P*). Given its particular effects on cell division and cell differentiation, we propose *UCN* to be a unique plant growth regulator. Interestingly, our combined genetic and biochemical evidence suggests that UCN suppresses ectopic growth in integuments through the direct negative regulation of the transcription factor ATS. *UCN* acts in a context-dependent fashion, because outgrowth formation in other tissues, such as filaments and petals, still occurs in *ucn ats* double mutants. Thus, *UCN* constitutes a general growth suppressor that interacts with additional, yet to be identified factors.

Our results provide unique insight into the mechanism controlling planar orientation of symmetric cell divisions in plants. *UCN* seems to play an important role in this process, because a periclinal or oblique cell division is the first discernible cellular defect in integument outgrowth of *ucn* mutants. A role in division plane control of symmetrically dividing cells is corroborated by the defect observed in *ucn* proembryos. UCN is unlikely to directly mediate the asymmetric subcellular localization of cellular factors, as it is known for some AGC VIII kinases (35). Rather, our evidence indicates that UCN acts in a more indirect fashion by modulating transcriptional programs via ATS to control planar growth of integuments.

The *ucn* phenotype and the interaction between *UCN* and *ATS* also provide evidence for the notion that maintenance of planar growth needs to be coordinated with adaxial–abaxial polarity during integument development. Class III HD-ZIP, KAN, and YABBY transcription factors play central roles in the establishment of adaxial–abaxial polarity in leaves (36, 37) and ovules (38), with *KAN* genes promoting abaxial cell fate and lamina outgrowth in leaves (26, 27). *ATS* is a *KAN* gene that regulates integument boundary formation, inner integument outgrowth, and adaxial–abaxial polarity (15, 28, 29, 38). A role for *UCN* in establishing adaxial–abaxial polarity in integuments is unlikely given the unaltered spatial expression pattern of several marker genes in *ucn*. Rather, our results raise the possibility that abnormal up-regulation of ATS activity in *ucn* within its normal expression domain interferes with planar growth control during integument extension. The results further indicate that maintaining planar growth requires the negative regulation of a factor involved in the control of adaxial–abaxial polarity. In this scenario, *UCN* would contribute to the coordination of these two processes. A defect in the coordination would result in ectopic growth, perhaps not unlike the instances in which loss of control of asymmetric cell division results in aberrant cell divisions (2).

Apart from the genetic antagonism between KAN and class III HD-ZIP genes in the establishment of organ polarity, nothing is known about the mechanism restricting KAN function (36, 37). Interestingly, our data imply that UCN acts as a direct negative regulator of a KAN transcription factor. Thus, it is possible that UCN-dependent planar growth control in other organs may involve the regulation of different KAN family members. Furthermore, the molecular process with which hyperactive ATS interferes in *ucn* integuments remains unknown. Considering these aspects, additional exploration of *UCN*-mediated signaling and its role in maintaining planar growth is needed.

Materials and Methods

Plant Work, Genetics, and Transformation. *Arabidopsis thaliana* (L.) Heynh. var. Columbia (Col-0) and var. Landsberg (*erecta* mutant) (L*er*), were used as wild-type strains. Plants were grown essentially as described (18).

Detailed information about all *ucn* and *ucnl* mutants identified in this study is given in *SI Appendix*, Table S2 and *SI Materials and Methods*. The *ucn-1* mutant was isolated previously in an ethane methyl sulfonate (EMS) mutagenesis (18) and outcrossed three times to L*er* before further analysis. The EMS-induced mutations *ucn-7* to *-10* were identified in the *UCN* CDS in a Col *er-105* background in conjunction with the Seattle *Arabidopsis* TILLING facility (39). The *ucn-2* and *-5* T-DNA insertion were predicted null alleles (*SI Appendix*, Fig. S3 *B* and *C* and Table S2). Moreover, in contrast to the other T-DNA lines, no wild-type *UCN* or *UCNL* transcripts, respectively, could be detected in these two mutants (*SI Appendix*, Fig. S5).

Plant transformation was performed by using the floral dip method (40).

Recombinant DNA Work. For DNA and RNA work, standard molecular biology techniques were used (41). PCR fragments used for cloning were obtained by using Phusion high-fidelity DNA polymerase (New England Biolabs). Site-directed mutagenesis of plasmids was done by using the QuikChange XL site-directed mutagenesis kit (Stratagene) according to the manufacturer's recommendations. All PCR-based constructs were sequenced. All primers used in this study are listed in *SI Appendix*, Table S5.

PCR-Based Gene Expression Analysis. To survey *UCN* and *UCNL* expression in plants, RNA from different organs was isolated by using the NucleoSpin RNA II kit (Macherey-Nagel). PCR was performed by using Taq DNA polymerase (New England Biolabs) and *UCN* and *UCNL*-specific primer pairs [UCN (sqRT)_F, UCN (sqRT)_R; UCNL (sqRT)_F, UCNL (sqRT)_R]. Between 19 and 32 thermal cycles were tested. The *GAPC* gene was used as positive control (42).

Tissue for qRT-PCR was harvested from 25-d-old plants grown in long-day conditions. With minor changes, tissue collection, RNA extraction, and quality control were performed as described (43). qRT-PCR was performed on a Roche LightCycler480 by using the iQ SYBR Green Supermix (Bio-Rad) according to the manufacturer's recommendations. By using the ΔΔ-Ct method, all gene expression levels were normalized against *At5g25760*, *At4g33380*, and *At2g28390* expression (44). Experiments were performed in biological and technical triplicates.

Generation, Expression, and Purification of Recombinant Proteins. All recombinant proteins were fusions of either a 6×-His/X-press (HIS) or a GST tag to the amino terminus of full-length UCN and ATS. Detailed cloning information is available from the authors upon request. The various constructs were transformed into *Escherichia coli* BL21 (DE3) cells (Invitrogen) and grown to an OD_{600} of 0.6. Recombinant protein expression was then induced by 0.5 mM isopropyl-β-D-thiogalactoside (FLUKA) for 4 h at 37 °C. Cells were pelleted and subjected to solubilization and recombinant protein purification by using the Protino Ni-TED 2000 (Macherey-Nagel) and Protino Glutathione Agarose 4B kits (GE Healthcare), respectively, according to the manufacturer's recommendations.

In Vitro Kinase Assays. Kinase assays were done with 4 μg of purified fusion protein and in the absence or presence of 2 μg of myelin basic protein (Sigma-Aldrich). Proteins were incubated in 20 μL of 40 mM Hepes (pH 7.4), 40 mM $MgCl_2$, 10 μM ATP, and 10 μCi [γ-^{32}P]ATP (Hartmann Analytic). The reaction was stopped by adding 5 μL of 4× sample buffer [100 mM Tris, pH 6.8, 20% (wt/vol) glycerol, and 4% (wt/vol) SDS]. The samples were boiled and analyzed by SDS-PAGE. Coomassie blue-stained gels were washed, dried, and exposed to Kodak film using an intensifying screen (Sigma).

Antibody Generation and Immunohistochemistry. Full-length recombinant HIS:UCN fusion protein purified from a SDS-PAGE gel was used to raise a polyclonal rabbit antiserum followed by IgG purification (Davids Biotechnologie). Goat anti-rabbit monoclonal antibody was coupled to Alexa-m488 (Invitrogen). Nuclei were stained with 1 mg/mL DAPI (Sigma). Antibody staining was performed as described (45) on the root tips of 6-d-old seedlings.

BiFC Assay. *UCN* and *ATS* coding sequences were PCR amplified and cloned into *pUC-SPYCE* and *pUC-SPYNE* vectors (46). The plasmid *pGY-1:mCherry* (47) was used as transformation control. Four micrograms of each plasmid in desired combinations was used to transiently transfect mesophyll protoplasts that were generated from 2-wk-old *Arabidopsis* leaves (Col) (48).

Microscopy, In Situ Hybridization, and Artwork. Preparation and analysis of samples for microscopy and histochemical localization of β-glucuronidase (GUS) activity in whole-mount tissue was done essentially as described (18, 49, 50). Confocal laser scanning microscopy was performed with an Olympus FV1000 setup and FluoView software (Olympus Europa) (*SI Appendix, SI Materials and Methods*). All images were obtained by sequential scanning to eliminate interference of lasers.

In situ hybridization with digoxigenin-labeled probes was done essentially as described (16). The *INO* and *PHB* probes were described (16). A 0.831-kb *ATS* antisense probe was obtained by PCR using a full-length cDNA clone (U8421; *Arabidopsis* Biological Resource Center) as template and the primer pair ATSas_831_F/ATSas_831_R. The sense control was obtained by using primer pair ATSsense_831_F/ATSsense_831_R. Slides were viewed with an Olympus BX61 upright microscope by using differential interference contrast optics. Images were adjusted for color and contrast by using Adobe Photoshop CS5 (Adobe) software.

ACKNOWLEDGMENTS. We thank C. Gasser for the *pINO::GUS* reporter line; G. Ingram, H. Tanaka, and M. Gruber for providing the *acr4-2*, *ale2-1*, and *sk21-D* mutants, respectively; the *Arabidopsis* Biological Resource Center (ABRC) for providing materials; A. Schnittger for advice on the cell-cycle genes; and S. Balasubramanian, J. Lohmann, and M. Hülskamp for comments on the manuscript. B.E. was supported by the Technische Universität München Graduate School Graduiertenzentrum Weihenstephan. This work was supported by Deutsche Forschungsgemeinschaft Grants LE 1265/3 and 1265/9 (to D.L.) and SCHN 723/3-1 and SCHN 723/3-2 (to K.S.).

1. Abrash EB, Bergmann DC (2009) Asymmetric cell divisions: A view from plant development. *Dev Cell* 16:783–796.
2. De Smet I, Beeckman T (2011) Asymmetric cell division in land plants and algae: The driving force for differentiation. *Nat Rev Mol Cell Biol* 12:177–188.
3. Rasmussen CG, Humphries JA, Smith LG (2011) Determination of symmetric and asymmetric division planes in plant cells. *Annu Rev Plant Biol* 62:387–409.
4. Tilney-Bassett RAE (1986) *Plant Chimeras* (E. Arnold, London).
5. Besson S, Dumais J (2011) Universal rule for the symmetric division of plant cells. *Proc Natl Acad Sci USA* 108:6294–6299.
6. Jenik PD, Irish VF (2000) Regulation of cell proliferation patterns by homeotic genes during *Arabidopsis* floral development. *Development* 127:1267–1276.
7. Schneitz K, Hülskamp M, Pruitt RE (1995) Wild-type ovule development in *Arabidopsis thaliana*: A light microscope study of cleared whole-mount tissue. *Plant J* 7:731–749.
8. Gifford ML, Dean S, Ingram GC (2003) The *Arabidopsis ACR4* gene plays a role in cell layer organisation during ovule integument and sepal margin development. *Development* 130:4249–4258.
9. Tanaka H, et al. (2007) Novel receptor-like kinase ALE2 controls shoot development by specifying epidermis in Arabidopsis. *Development* 134:1643–1652.
10. Watanabe M, Tanaka H, Watanabe D, Machida C, Machida Y (2004) The ACR4 receptor-like kinase is required for surface formation of epidermis-related tissues in *Arabidopsis thaliana*. *Plant J* 39:298–308.
11. Colombo L, Battaglia R, Kater MM (2008) Arabidopsis ovule development and its evolutionary conservation. *Trends Plant Sci* 13:444–450.
12. Kelley DR, Gasser CS (2009) Ovule development: genetic trends and evolutionary considerations. *Sex Plant Reprod* 22:229–234.
13. Robinson-Beers K, Pruitt RE, Gasser CS (1992) Ovule development in wild-type Arabidopsis and two female-sterile mutants. *Plant Cell* 4:1237–1249.
14. Balasubramanian S, Schneitz K (2000) *NOZZLE* regulates proximal-distal pattern formation, cell proliferation and early sporogenesis in *Arabidopsis thaliana*. *Development* 127:4227–4238.
15. McAbee JM, et al. (2006) *ABERRANT TESTA SHAPE* encodes a KANADI family member, linking polarity determination to separation and growth of Arabidopsis ovule integuments. *Plant J* 46:522–531.
16. Sieber P, et al. (2004) Pattern formation during early ovule development in *Arabidopsis thaliana*. *Dev Biol* 273:321–334.
17. Skinner DJ, Gasser CS (2009) Expression-based discovery of candidate ovule development regulators through transcriptional profiling of ovule mutants. *BMC Plant Biol* 9:29.
18. Schneitz K, Hülskamp M, Kopczak SD, Pruitt RE (1997) Dissection of sexual organ ontogenesis: A genetic analysis of ovule development in *Arabidopsis thaliana*. *Development* 124:1367–1376.
19. McConnell JR, et al. (2001) Role of *PHABULOSA* and *PHAVOLUTA* in determining radial patterning in shoots. *Nature* 411:709–713.
20. Villanueva JM, et al. (1999) INNER NO OUTER regulates abaxial-adaxial patterning in Arabidopsis ovules. *Genes Dev* 13:3160–3169.
21. Smith LM, Bomblies K, Weigel D (2011) Complex evolutionary events at a tandem cluster of *Arabidopsis thaliana* genes resulting in a single-locus genetic incompatibility. *PLoS Genet* 7:e1002164.
22. Bögre L, Okrész L, Henriques R, Anthony RG (2003) Growth signalling pathways in *Arabidopsis* and the AGC protein kinases. *Trends Plant Sci* 8:424–431.
23. Galván-Ampudia CS, Offringa R (2007) Plant evolution: AGC kinases tell the auxin tale. *Trends Plant Sci* 12:541–547.
24. Hirt H, Garcia AV, Oelmüller R (2011) AGC kinases in plant development and defense. *Plant Signal Behav* 6:1030–1033.
25. Zhang Y, McCormick S (2009) AGCVIII kinases: At the crossroads of cellular signaling. *Trends Plant Sci* 14:689–695.
26. Eshed Y, Baum SF, Perea JV, Bowman JL (2001) Establishment of polarity in lateral organs of plants. *Curr Biol* 11:1251–1260.
27. Kerstetter RA, Bollman K, Taylor RA, Bomblies K, Poethig RS (2001) *KANADI* regulates organ polarity in *Arabidopsis*. *Nature* 411:706–709.
28. Balasubramanian S, Schneitz K (2002) *NOZZLE* links proximal-distal and adaxial-abaxial pattern formation during ovule development in *Arabidopsis thaliana*. *Development* 129:4291–4300.
29. Léon-Kloosterziel KM, Keijzer CJ, Koornneef M (1994) A seed shape mutant of *Arabidopsis* that is affected in integument development. *Plant Cell* 6:385–392.
30. Gao P, et al. (2010) A new dominant *Arabidopsis transparent testa* mutant, *sk21-D*, and modulation of seed flavonoid biosynthesis by KAN4. *Plant Biotechnol J* 8: 979–993.
31. Hunter CT, et al. (2012) *Cellulose Synthase-Like D1* is integral to normal cell division, expansion, and leaf development in maize. *Plant Physiol* 158:708–724.
32. Motose H, Tominaga R, Wada T, Sugiyama M, Watanabe Y (2008) A NIMA-related protein kinase suppresses ectopic outgrowth of epidermal cells through its kinase activity and the association with microtubules. *Plant J* 54:829–844.
33. Reynolds JO, Eisses JF, Sylvester AW (1998) Balancing division and expansion during maize leaf morphogenesis: Analysis of the mutant, *warty-1*. *Development* 125: 259–268.
34. Kessler S, Seiki S, Sinha N (2002) *Xcl1* causes delayed oblique periclinal cell divisions in developing maize leaves, leading to cellular differentiation by lineage instead of position. *Development* 129:1859–1869.
35. Dhonukshe P, et al. (2010) Plasma membrane-bound AGC3 kinases phosphorylate PIN auxin carriers at TPRXS(N/S) motifs to direct apical PIN recycling. *Development* 137: 3245–3255.
36. Husbands AY, Chitwood DH, Plavskin Y, Timmermans MC (2009) Signals and prepatterns: New insights into organ polarity in plants. *Genes Dev* 23:1986–1997.
37. Szakonyi D, Moschopoulos A, Byrne ME (2010) Perspectives on leaf dorsoventral polarity. *J Plant Res* 123:281–290.
38. Kelley DR, Skinner DJ, Gasser CS (2009) Roles of polarity determinants in ovule development. *Plant J* 57:1054–1064.
39. Till BJ, et al. (2003) Large-scale discovery of induced point mutations with high-throughput TILLING. *Genome Res* 13:524–530.
40. Clough SJ, Bent AF (1998) Floral dip: a simplified method for *Agrobacterium*-mediated transformation of *Arabidopsis thaliana*. *Plant J* 16:735–743.
41. Sambrook J, Fritsch EF, Maniatis T (1989) *Molecular Cloning* (Cold Spring Harbor Lab Press, Plainview, NY).
42. Shih MC, Heinrich P, Goodman HM (1991) Cloning and chromosomal mapping of nuclear genes encoding chloroplast and cytosolic glyceraldehyde-3-phosphate-dehydrogenase from *Arabidopsis thaliana*. *Gene* 104:133–138.
43. Box MS, Coustham V, Dean C, Mylne JS (2011) Protocol: A simple phenol-based method for 96-well extraction of high quality RNA from Arabidopsis. *Plant Methods* 7:7.
44. Czechowski T, Stitt M, Altmann T, Udvardi MK, Scheible WR (2005) Genome-wide identification and testing of superior reference genes for transcript normalization in Arabidopsis. *Plant Physiol* 139:5–17.
45. Völker A, Stierhof YD, Jürgens G (2001) Cell cycle-independent expression of the *Arabidopsis* cytokinesis-specific syntaxin KNOLLE results in mistargeting to the plasma membrane and is not sufficient for cytokinesis. *J Cell Sci* 114:3001–3012.
46. Walter M, et al. (2004) Visualization of protein interactions in living plant cells using bimolecular fluorescence complementation. *Plant J* 40:428–438.
47. Hoefle C, et al. (2011) A barley ROP GTPase ACTIVATING PROTEIN associates with microtubules and regulates entry of the barley powdery mildew fungus into leaf epidermal cells. *Plant Cell* 23:2422–2439.
48. Yoo SD, Cho YH, Sheen J (2007) Arabidopsis mesophyll protoplasts: A versatile cell system for transient gene expression analysis. *Nat Protoc* 2:1565–1572.
49. Gross-Hardt R, Lenhard M, Laux T (2002) *WUSCHEL* signaling functions in interregional communication during *Arabidopsis* ovule development. *Genes Dev* 16: 1129–1138.
50. Torres-Ruiz RA, Jürgens G (1994) Mutations in the *FASS* gene uncouple pattern formation and morphogenesis in *Arabidopsis* development. *Development* 120: 2967–2978.
51. Cutler SR, Ehrhardt DW, Griffitts JS, Somerville CR (2000) Random GFP:cDNA fusions enable visualization of subcellular structures in cells of *Arabidopsis* at a high frequency. *Proc Natl Acad Sci USA* 97:3718–3723.